Appendices

Appendix Table of Contents

APPENDIX 2 – CELL CULTURE OPTIMIZATION

Background

Primary hippocampal cell culture as a model of AD

In this work, numerous experiments were conducted using low-density cultures of primary, embryonic hippocampal cells to which monomeric $A\beta_{42}$ or AβOs were applied as a model of AD. Unlike clonal cell lines, primary cells in culture have the advantage of naturally forming differentiated axons and dendrites with extensive synaptic connections[68,69]. At low density, the neurons form a monolayer over which individual dendrites can be distinguished and individually analyzed. Additionally, hippocampal cell cultures prepared from late embryonic tissue contain a relatively uniform population mostly comprised of pyramidal neurons, with low levels of glial cells. These cultures, which are most often prepared from rat embryonic tissue, are well-characterized in the literature. Hippocampal cells were also preferred because, at very early stages in AD, neurodegeneration is observed in the hippocampus[70]. Hippocampal cells also exhibit high levels of binding to AβOs in culture, and resulting calcium dyshomeostasis, oxidative stress, tau phosphorylation, and synaptotoxicity have been observed[71-74]. As such, biological mechanisms of AβO formation, neurodegeneration, and binding can be investigated using this model.

Methods for culture hippocampal cells

Two predominant methods have been established for the culture of primary hippocampal neurons. One, established by Banker et al., involves sandwich co-cultures of neurons with an astrocyte feeder layer, which provide the necessary neurotrophic factors to support the growth of low-density cell cultures[68,75]. After maturation, coverslips containing neurons can then be

separated from the astrocyte feeder layer for experimental use. A second protocol, developed by Brewer et al., involves growth of neurons in a defined, serum-free medium which supplies trophic factors and suppresses the growth of glial cells[75-77]. This enables growth of neurons with minimal glial cells that can be directly used for cell culture without transfer. The protocol used here is based on this method.

Procedure

Nitric acid wash coverslips (≥2 days, non-sterile)

1. Add 12 mm coverslips (Fisher Scientific 12-545-80P or 12-545-81P) to a rectangular glass dish with a lid.
2. In a fume hood, carefully add concentrated nitric acid (Fisher Scientific A200-500) to the glass dish with coverslips.
3. Place the coverslips in nitric acid on an orbital shaker for ≥24 h with the lid on.
4. After 24 h, vent the coverslip container in the fume hood briefly. Then, dispose of nitric acid by decanting slowly, diluting into a high volume of cold water for disposal.
    - It is normal for this step to generate heat. Use plenty of cold water to mitigate heat.
5. Rinse once quickly with reverse-osmosis water to the dish.
6. Perform 6 washes, for ≥1 h each, with double-distilled (dd)H_2O on an orbital shaker.
    - For this step, shaker speed should be rapid enough that coverslips are moving slightly within the glass dish.
7. After washes, lay coverslips out individually on large, clean pieces of paper to dry, approximately 2-3 h.
    - To avoid accumulation of dust, coverslips cannot be left to dry overnight in this step.

8. Transfer coverslips to clean glass Petri dishes.
    - Nitric acid-washed coverslips can collect dust over time after cleaning. For this reason, it is best to prepare freshly-coated coverslips at least every 2-3 months.

Coating coverslips with poly-D-lysine (1 day, sterile)

Autoclave in advance: forceps, non-cotton-plugged glass pipettes, two 500 mL glass bottles containing ddH_2O.

1. Using sterile forceps, fill 4-5 plastic Petri dishes (100 mm) with a single layer of coverslips (about 35-40 coverslips in each).
2. Prepare the poly-D-lysine (PDL) stock (5 mg PDL (Sigma-Aldrich P6407) + 50 mL sterile ddH_2O), or thaw a prepared solution at 37 °C.
3. Prepare the PDL working solution by 1:1 dilution of PDL stock with sterile ddH_2O, invert several times to mix.
4. Add 10 mL of the PDL working solution to each dish.
    - Some coverslips will float up from the bottom. Use a sterile glass pipet to push each coverslip down to the bottom of the dish with minimal overlap.
5. Incubate the coverslips in this solution in a sterile hood for 1 h at RT.
6. Wash the coverslips 4 times with 20 mL sterile ddH_2O per wash and 45 min each on an orbital shaker.
    - After adding water, use a glass pipet each time to make sure the coverslips lay flat, non-overlapping, at the bottom again.
7. Using sterile forceps, transfer the coverslips into 35 mm sterile dishes, 4 coverslips per dish. Ensure that the coverslips do not touch one another or the edges of the dish.

8. Allow these dishes with coverslips to dry overnight.
    - The coated coverslips may be used as soon as the next day and should not be stored for more than 1 week. Coverslips must be kept in a sterile environment until use.

Tissue dissection and dissociation and neuron plating (1 day, sterile)

Prepare in advance: In advance, prepare and store 680 mM glutamate stock (0.2 g L-glutamate (Calbiochem 3510) + 2 mL 2M HCl) stored at 4 °C. Fire-polish cotton-plugged glass pipettes. Autoclave: dissecting forceps, one 150 mL glass bottle, and the box of fire-polished pipettes. Obtain a new lab coat to use for each new cell culture. Measure 6 mg papain (Sigma-Aldrich P4762) into a 15 mL tube, and store this at -20 °C until use. Clean 1-2 plastic trays, sterilize them with ethanol, and keep them in a sterile environment until use.

Prepare the same day: Prepare the hippocampal plating media (25 μM glutamate in NbActiv1): 3.68 μL glutamate stock + 100 mL NbActiv1 (Transnetyx NB1), sterile filter and store at room temperature until use. Warm at room temperature: Hibernate E (-$CaCl_2$) (Transnetyx HECA) and nigrosin stain (0.3% w/v in HBSS). Turn on a heat sterilizer and allow it to reach 200 °C prior to use.

1. Prepare the cell dissociation solution (3 mL Hibernate E(-$CaCl_2$) + 6 mg papain), incubate it 10 min at 37 °C, and sterile-filter it prior to use.
2. Dissect hippocampus, leaving a small amount of cortex attached.
    - Use a sterilizing heater to ensure sterility of forceps prior to dissecting.
3. Using cotton-plugged pipettes, remove most of the original Hibernate EB complete (HEB, Transnetyx HEB) solution, leaving all the tissue at the bottom of the tube in a low volume of media.

4. Add 2 mL of the sterile cell dissociation solution to the tissue, incubate this 10 min (must be less than 20 min) at 37 °C. Invert once to mix halfway though.
5. Remove most of the cell dissociation solution, leaving the tissue at the bottom of the tube.
6. Add the original HEB solution back to the tissue to neutralize it.
7. Triturate the tissue 10 times maximum using a sterile, fire-polished, cotton-plugged glass pipet.
8. Centrifuge the tube containing tissue 1100 (200 x g) for 2 min. A small, defined pellet should form.
9. Remove the HEB solution, leaving a minimal volume of media containing the pellet in the tube.
10. Add 2 mL of the plating media to the tissue. Triturate the tissue 10 times maximum to resuspend it.
11. In a small tube, mix 180 µL of 0.3% nigrosin in HBSS solution with 20 µL of the cell solution and vortex. Then, add 10 µL of this solution to each side of a hemocytometer to count the cells.
    - The total number of cells counted here should be ≥100.
    - Calculate the concentration of cells based on the following parameters: (1) volume of each of 5 large squares on the hemocytometer is 0.1 mm^3 = 0.0001 mL, (2) 1:10 dilution of cells into vital dye. Apply the equation:

$$\frac{avg.\ \#\ cells\ per\ square}{volume\ of\ square\ (0.0001\ mL)} \times \frac{vol.\ counting\ solution\ (200\ \mu L)}{vol.\ cell\ solution\ added\ (20\ \mu L)} = number\ \frac{total\ millions\ cells}{mL\ cell\ solution}$$

    which can be simplified to:

$$\frac{Avg.\#\ cells\ per\ square}{10} = number\ \frac{total\ millions\ cells}{mL\ cell\ solution}$$

12. Add additional plating media to dilute the cell solution to the desired concentration (110,000 cells/mL) and invert 3 times to mix.
13. Arrange the 35 mm dishes containing coverslips in a clean, sterile plastic tray.
14. Plate the cells directly onto each coverslip, 150 uL on each coverslip. The cell suspension should form a bead on top of the coverslip.
    - This plating volume produces a cell density of approximately 15,000/cm^2:

$$\frac{110{,}000\ cells}{mL} \times \frac{0.15\ mL}{coverslip} \times \frac{coverslip}{(6mm)^2\pi} \times \left(\frac{10\ mm}{cm}\right)^2 = 14{,}589\ {}^{cells}/_{cm^2}$$

15. Cover the tray with a lid, and carefully place the tray into the incubator. Allow the cells to attach at 37 °C, 5% CO_2, for 45 min-1 h.
16. Use a microscope to verify that the cells have attached to the coverslips, and capture images before feeding.
17. Add 1.4 mL of the plating media to each dish to a final volume of 2 mL, filling the dish.
18. Return the tray to the incubator, and incubate the cells 37 °C, 5% CO_2.

Feeding cells (sterile, feed cells on day 4, then every 3 days, 2 h per day)

Prepare the same day/in advance: Prepare 7 sterile aliquots of NbActiv1 media according to the volume needed to feed the culture, approximately 45 mL. Warm NbActiv1 to 37 °C.

1. First, image 5 coverslips under the microscope, as a record of cell growth.
2. Feed all the dishes by half-media exchange.
    - Remove 1 mL of old media from each dish and dispose. Add 1 mL of fresh NbActiv1 back to each dish. Use a new pipet tip each time.
    - Note: ensure all pipetting is done slowly and carefully to avoid disturbing the cells. The pipet tip should touch the dish, but not the coverslips.

3. Return the tray of cells to the incubator at 37 °C, 5% CO_2.

Results and discussion

In this work, 60 neuron cultures were conducted. Kirsten Viola provided significant advice and conducted the tissue dissections, and Yifan Xu and Weijian Huang assisted with several cell cultures and contributed to optimization. Optimization of cultures grown on glass coverslips and 96-well plates will be described. Overall, primary hippocampal neuron culture was healthiest when some cortical cells were included for neurotrophic support, and when cells were triturated using fire-polished pipets, plated on poly-D-lysine coated glass coverslips, at a density of 0.11-0.22 million cells/mL (15,000-30,000 cells/cm^2) (Figure 1).

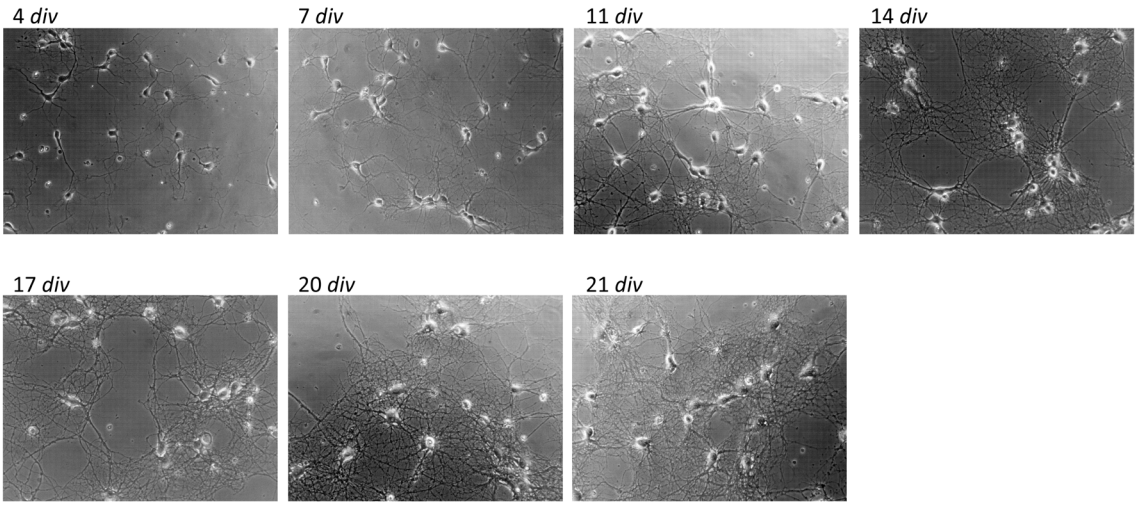

Figure A2.1 Healthy neuronal cells in culture. Representative images of healthy neuronal cells in culture from 4 *div* to 21 *div* are shown. Cells were used for experiments between 18-25 *div.*

Optimal coverslip coating was obtained with poly-D-lysine

Initially, neurons were grown using pre-dissected hippocampal tissue sourced from BrainBits; initial optimization used this tissue. Optimization of coverslip coating demonstrated

that poly-D-lysine (PDL) enabled superior survival at 3 *div* when compared to poly-L-lysine, and coverslips washed four times instead of once after incubation with PDL also appeared to demonstrate better distribution and survival of neurons overall (Figure 2). This is in agreement with the theoretical advantage that poly-D-lysine is a non-bioactive enantiomer, whereas poly-L-lysine, the naturally occurring enantiomer, and can cause toxicity to cells[78]. However, several studies have used poly-L-lysine as a substrate without toxicity to neurons[68]. The results obtained here indicate that poly-D-lysine was preferable for neuronal attachment under the conditions tested here.

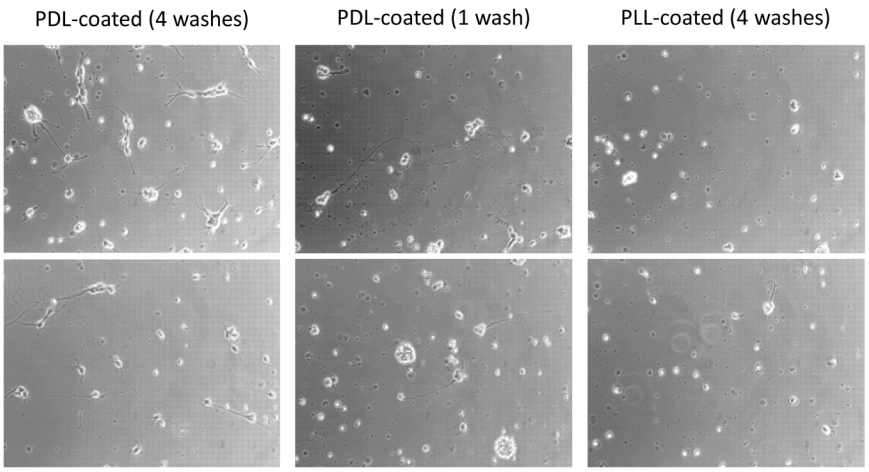

Figure A2.2 Poly-D-lysine coating yielded best survival. Two representative images each are presented of 3 *div* cultures grown on coverslips prepared with three different coating conditions. The leftmost set was coated with poly-D-lysine (PDL) and washed 4x prior to use. The center set was coated with PDL and washed just 1x prior to use. The rightmost set was coated with poly-L-lysine and washed 4x prior to use.

"Rough" dissection and sufficient media volume yielded healthier cells with increased survival

At the recommendation of Kirsten Viola, the dissection process was next optimized by including a small amount of cortical tissue in a "rough" dissection of hippocampus. This "rough" dissection dramatically improved culture quality, producing healthier cells and survival of

neurons to older ages (Figure 3). These results match a significant body of literature supporting the neurotrophic effect of astrocytes in neuronal cell culture[79].

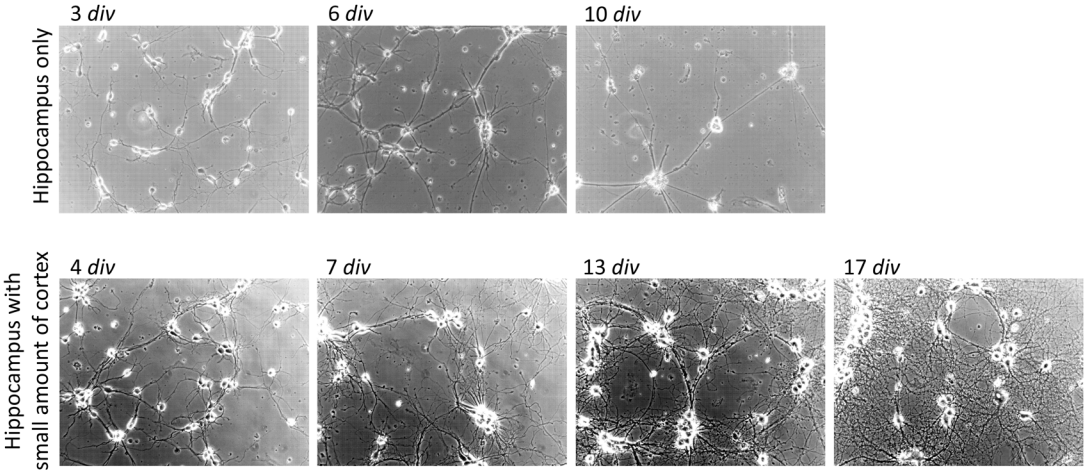

Figure A2.3 Healthier cells with longer survival were obtained when a small amount of cortex was included. Representative images of cells grown in culture with or without a small amount of cortex included. Cultures of hippocampus only (top) tend to clump together, and severe damage is observed by 10 *div*. Cultures of hippocampus with a small amount of cortex can survive beyond 17 *div* and form better distributed cultures which make a network of fine processes. Cells are from two different cultures and were imaged on different days, but the same general trend was observed in at least 3 cultures for each condition.

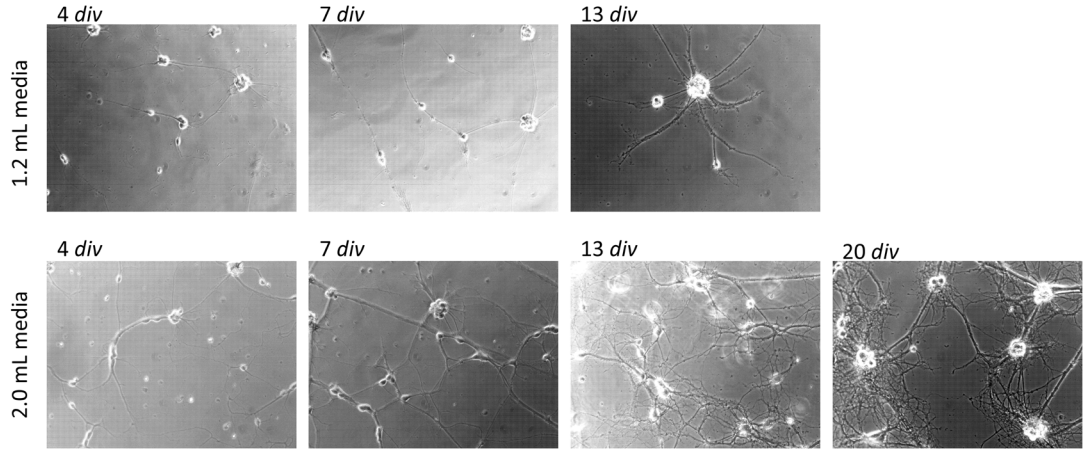

Figure A2.4 Use of sufficient media volume (2mL) was necessary for neuronal health and longevity. Representative images of cells grown in cultures with different volumes of media. Cultures with 2.0 mL media (in 35 mm dishes) survived longer and were healthier than cultures in 1.2 mL media. Cultures were grown on different days from different tissue, but 2 mL of media consistently yielded healthy cultures.

Optimization of the media volume demonstrated that 2.0 mL media yielded healthier cells and longer survival than 1.2 mL (Figure 4). This volume, in the 35 mm dish, is likely needed to enable sufficient nutrition over the intervals over which media is unchanged.

Fire-polishing pipettes and reducing cell concentration improved cell dispersal

Trituration with fire-polished pipettes also yielded slightly improved cell dispersal compared to untreated pipettes (Figure 5). This effect could be attributed to reduced damage of cells during trituration due to the smoother surface of the pipet, or to the slight narrowing of the pipette opening that is achieved by fire-polishing, enabling more thorough cell dissociation.

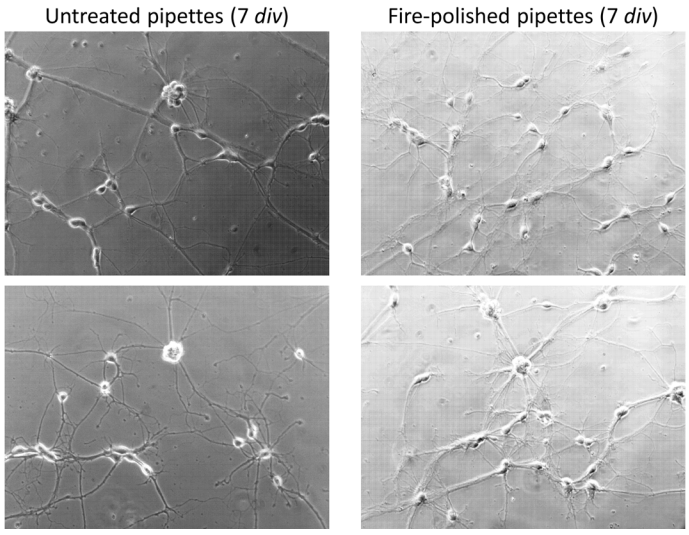

Figure A2.5 Fire-polishing pipettes yielded slightly improved dispersal of cells early in culture. Representative images of cells at 7 *div* in cultures dispersed by trituration with untreated pipettes (left) versus fire-polished pipettes (right). Although cultures were similar, use of fire-polished pipettes appeared to yield better dispersal of cells with reduced clumping at 7 *div*. Images are from different cultures prepared with different tissues, but use of fire-polished pipettes for subsequent cultures consistently yielded healthy, well-distributed cells.

Finally, using a lower concentration of cells (15,000 vs 30,000 cells/cm^2) did not harm cell survival or health, and in fact slightly reduced cell clumping (Figure 6). Additionally, this concentration enabled production of twice as many of coverslips, thereby doubling the number of experiments that could be conducted. Therefore, these combined optimized conditions were used

for all future cell cultures. Although these cells were most often healthiest around 21 *div*, when they were typically used in experiments, they could live longer, even up to 36 *div (*Figure 7).

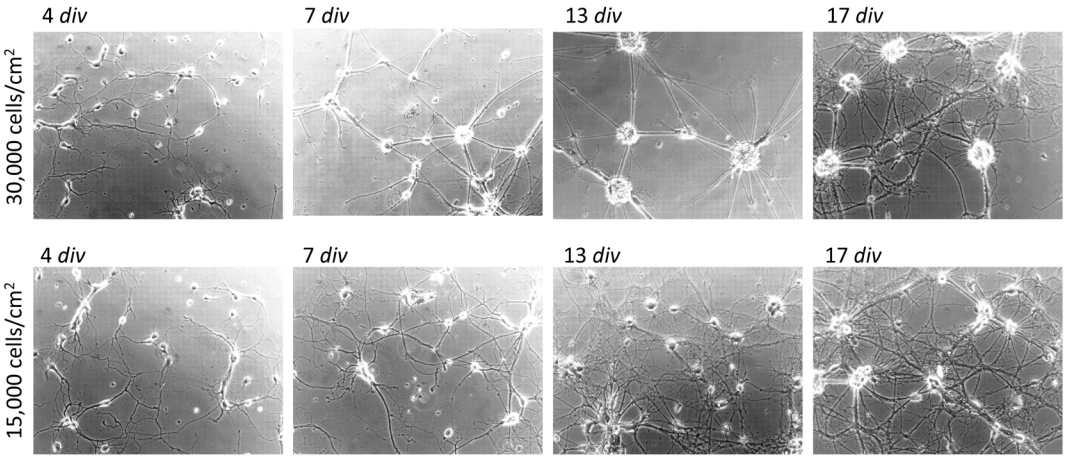

Figure A2.6 Cells grown at 0.11 million/mL are healthy with slightly improved distribution later in culture. Representative images of cells at 4-17 *div* in cultures plated at 30,000 cells/cm^2 (top) versus 15,000 cells/cm^2 (bottom). Lower concentrations appeared to yield better dispersal of cells at older ages in culture. These cultures were prepared from the same tissue on the same day. After this time, cells plated at 15,000 cells/cm^2 over numerous cultures demonstrated good health and dispersal.

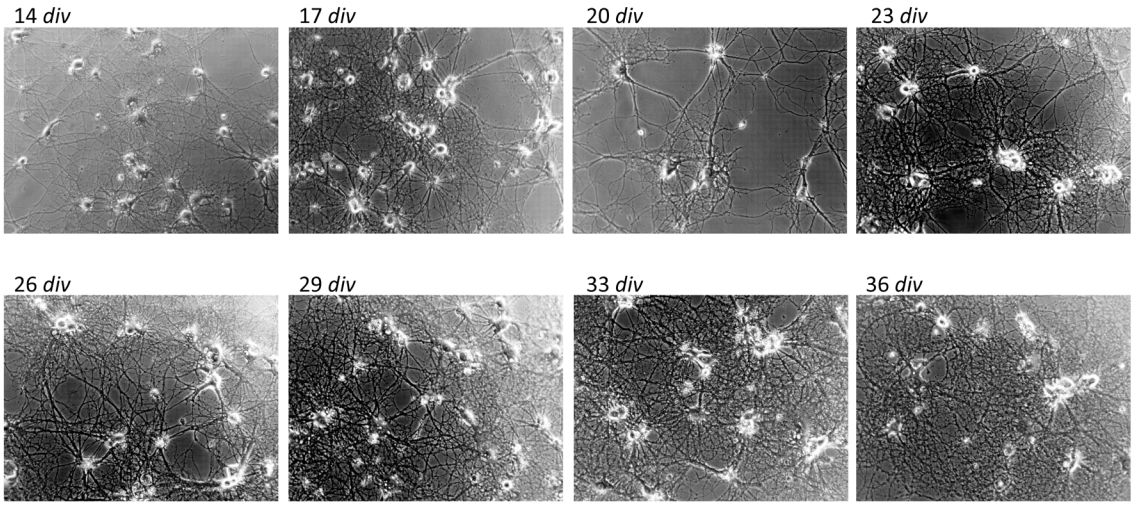

Figure A2.7 Extended survival of cells in culture. Representative images of cells at 14-36 *div* in culture.

Use of trays without lids reduced survival

An additional experiment tested the viability of growing cells within dishes placed in glass trays without lids, which had the benefit of being autoclavable, and therefore more sterile. However, in glass trays, survival of cells was dramatically reduced compared to the previously used plastic trays with lids (Figure 8). The lid may protect against contamination or maintain a favorable local humidity or gas environment around the dishes. Based on the results of this experiment, plastic trays with lids were continued in use after this test.

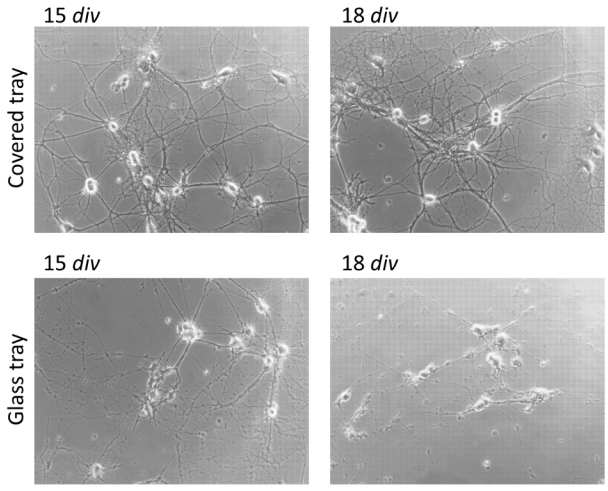

Figure A2.8 Reduced survival in glass tray compared to covered tray. Representative images of cells at 15 and 18 *div* in culture dishes incubated within a covered tray (top) versus a glass tray without a lid (bottom).

Healthy neurons were grown on 96-well plates

A handful of cell cultures were also conducted on 96-well plates for use in live-cell assays. Optimized conditions included plating media without glutamate (Figure 9), density of 20,000-40,000 cells per well, and use of Greiner pre-coated plates (Figure 10). These conditions yielded the healthiest cultures among those grown on plates. Overall, the cells grown on coverslips were healthier than those grown on plates. However, growth of neurons in 96-well

plates was a valuable tool for live-cell, high-throughput assays in which high-magnification microscopy was not needed.

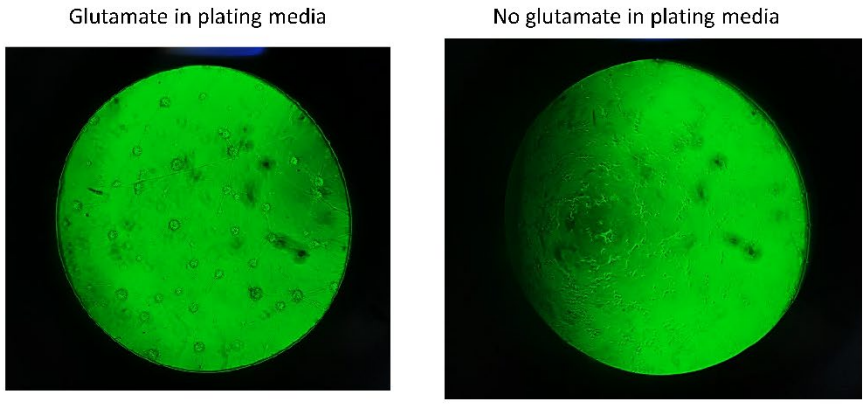

Figure A2.9 Cells in plates grown without glutamate clumped less. Cells were grown in pre-coated 96-well plates, plated either in NbActiv4 media with (left) or without (right) glutamate, and were imaged at 7 *div.* Both conditions were cultured at the same time from the same tissue. Cells plated without glutamate in the plating media were less clumped.

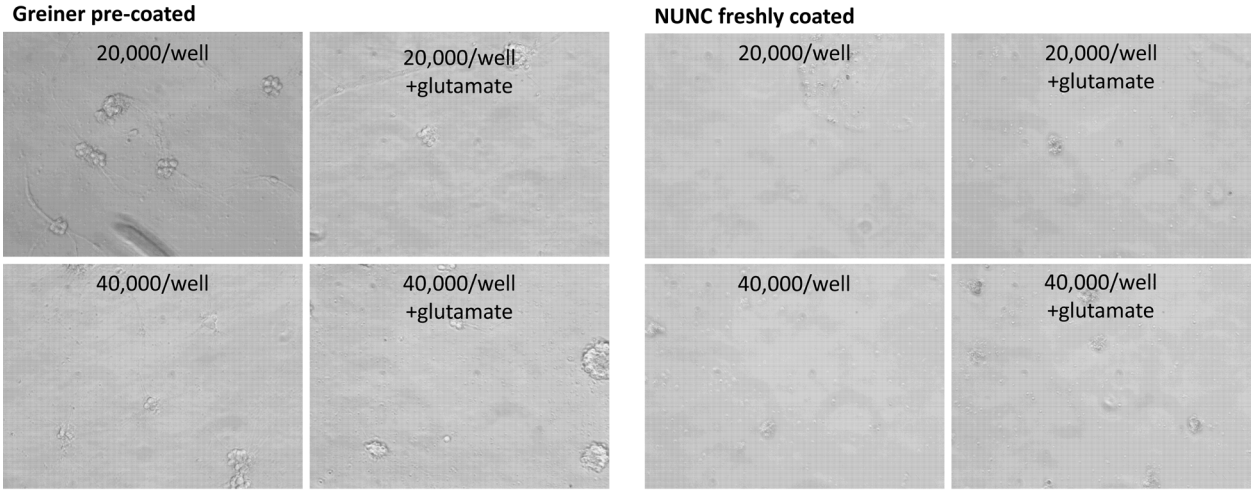

Figure A2.10 Cells survived in moderate health at 20,000-40,000 cells/well in Greiner pre-coated plates. Cells grown in Greiner pre-coated 96-well plates (left panel) or NUNC, freshly coated plates (right panel), and plated at 20,000-40,000 cells/well in the presence or absence of glutamate were imaged at 14 *div*. Cells in the Greiner plates survived to 14 *div,* while those in the freshly coated plate did not survive. This is attributed to excess PDL in the wells, which is difficult to remove from plastic by washing. Within the Greiner plate, the cells grown in the absence of glutamate demonstrate the most elongated processes with the least clumping.

Coverslip cultures demonstrated differentiated axons and robust AβO binding

Cells grown on coverslips using the optimized procedure developed differentiated axons and dendrites in culture at 14 *div* (Figure 11). These were demonstrated by immunofluorescent labeling of the dendrite-specific microtubule-associated protein 2 (MAP2) and the axon-specific tau protein[80]. The very modest presence of tau signal in dendrites that was observed in the dendrites in this experiment is typical of cells grown in culture, as seen in the experiments of Zempel et al[81].

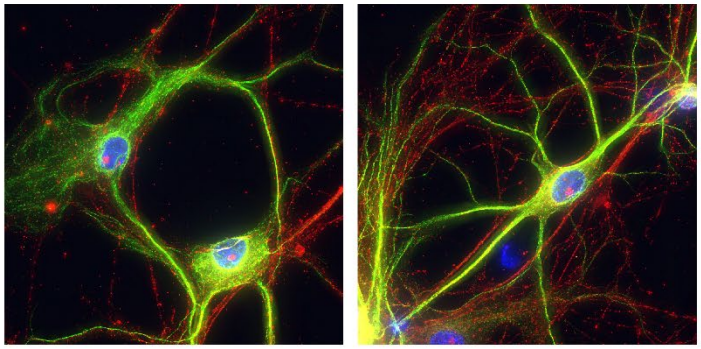

Figure A2.11 Neurons in culture demonstrated differentiated axons and dendrites. Two representative images from cells grown on coverslips according to the optimized procedure. At 14 *div*, axons and dendrites were labeled with antibodies against tau protein (red) and microtubule-associated protein 2 (green), respectively.

Further, to determine whether neurons grown with these methods could bind AβOs, crosslinked AβOs made according to the procedure of Cline et al. were applied (500 nM, 30 min) to neurons in culture at 20 *div*[82]. AβOs were labeled by immunofluorescence using the in-house antibody NU-2 and dendrites were labeled with an antibody against MAP2. Binding of AβOs was clearly observed along dendrites of cells in these cultures (Figure 12).

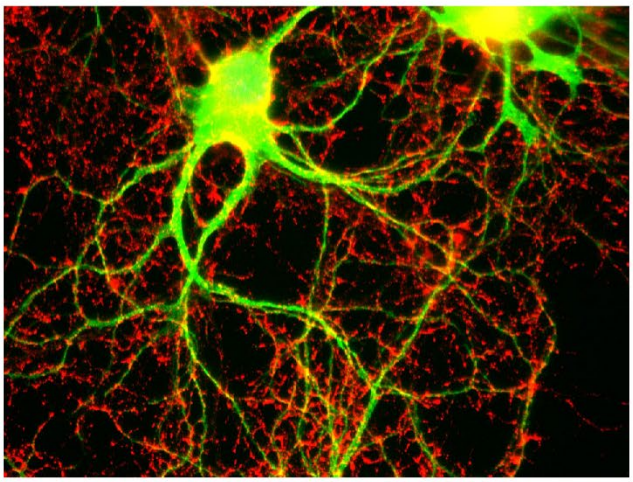

Figure A2.12 Dendritic binding of AβOs was clearly detected in hippocampal neuron culture. Representative image of hippocampal neurons grown on coverslips according to the optimized procedure. Binding of crosslinked AβOs (NU2, red) along dendrites (MAP2, green) can be clearly observed.

Conclusion

Optimization of primary hippocampal neuron culture resulted in a protocol in which a small amount of cortical tissue was included to provide neurotrophic support, trituration was conducted using fire-polished pipets to improve dispersal, coverslips were coated with poly-D-lysine, and cells were plated at a density of 15,000-30,000 cells/cm^2. These conditions were used to reproducibly grow healthy cultures. In these cultures, axons and dendrites were differentiated by 14 *div* and AβO binding was robustly detected in experiments conducted at 20 *div*.

APPENDIX 3 - IMAGEJ MACROS

Save open files

The macro written below saves all open files as .tif files. Most files are saved from the microscope as proprietary, .lif files, therefore this macro is used to save tiffs for all open files for further processing.

```
for (i=1; i<=nImages; i++) {
     selectImage(i);
     title = getTitle();
     saveAs("tiff","[filepath]"+title);
close();
}
```

Random nameS

Instead of a macro, the .bat file “Random Names”, written by Jason Faulkner (https://www.howtogeek.com/57661/stupid-geek-tricks-randomly-rename-every-file-in-a-directory/), was used to randomly name the tiffs, to enable blind analysis.

Save open files specific channels

The macro written below saves the red and green channels of each open image into the designated folders in the macro.

```
for (i=1; i<=nImages; i++) {
     selectImage(i);
     title = getTitle();
     run("Select All");
     run("Duplicate...", "duplicate channels=1");
     saveAs("tiff", "[filepath]/Red/"+title);
close();
     run("Duplicate...", "duplicate channels=2");
     saveAs("tiff", "[filepath]/Green/"+title);
close();
     //run("Duplicate...", "duplicate channels=3");
     //saveAs("tiff", "[filepath]/Blue/"+title);
//close();
close();
}
```

Use dendrites and analyze length

The following macro was used to analyze the total length of the dendrite skeleton, in each image, in microns. These values are reported using the print function as [filename]__[total_length]. During the operation of the macro, the user specifies one folder as an input for the dendrite signal, and one folder for the output of the shape of the dendrite skeleton. The threshold used for MAP2 in this macro is set by default to 15 but was tested and set for each experiment at an appropriate value that was kept constant within the analysis of that experiment.

```
inputMAP2 = getDirectory("Choose Input MAP2 Directory");
//inputnucleus = getDirectory("Choose Input Nucleus Directory");
//outputdendrites = getDirectory("Choose Output Dendrites Directory");
outputskeleton = getDirectory("Choose Output Skeleton Directory");

function skeleton(inputMAP2, outputskeleton, filename)
{
//Create skeleton
      open(inputMAP2 + filename);
      run("Gaussian Blur...", "sigma=2");
      setThreshold(15, 255);
      setOption("BlackBackground", false);
      run("Convert to Mask");
      run("Skeletonize");
      saveAs("Tiff", outputskeleton + "/" + filename);
//Analyze the skeleton and save the total length
      run("Analyze Skeleton (2D/3D)", "prune=none show");
      close("Results");
      Table.rename("Branch information", "Results");
      for(i=0; i<nResults; i++) {
            total_length += getResult("Branch length", i);
    }
print(filename + "__" + total_length);
      close("*");
      close("Results");
}

setBatchMode(true);
list = getFileList(inputMAP2);
for (i = 0; i < list.length; i++)
        skeleton(inputMAP2, outputskeleton, list[i]);
setBatchMode(false);
```

Use dendrites to analyze NU2

The following macro was used to analyze the number of NU2 puncta above the selected threshold within a region around the dendrites. During the operation of the macro, folders are specified for the input images in two channels, as well as an output of the area that was tested. As in the previous macro, the threshold used for MAP2 in this macro is set by default to 15 but was tested and set for each experiment at an appropriate value that was kept constant within the analysis of that experiment.

```
inputdendrites = getDirectory("Choose Input Dendrite Directory");
inputNU2 = getDirectory("Choose Input NU2 Directory");
outputarea = getDirectory("Choose Output Area Directory");
NU2_threshold = getNumber("Choose a threshold for NU2", 50);

function analyze_NU2(inputdendrites, inputNU2, outputarea,
NU2_threshold, filename)
{
//Use dendrites to identify analysis area
      open(inputdendrites + filename);
      run("Gaussian Blur...", "sigma=2");
      setThreshold(35, 255);
      setOption("BlackBackground", false);
      run("Convert to Mask");
      run("Options...", "iterations=15 count=1 do=Dilate");
      saveAs("Tiff", outputarea + "/" + filename);
      run("Create Selection");
      close();
//Analyze particles in NU2
      open(inputNU2 + filename);
      run("Restore Selection");
      setThreshold(NU2_threshold, 255);
      run("Analyze Particles...", "display summarize");
      close();

}

setBatchMode(true);
list = getFileList(inputdendrites);
for (i = 0; i < list.length; i++)
        analyze_NU2(inputdendrites, inputNU2, outputarea,
NU2_threshold, list[i]);
setBatchMode(false);
```

References (Appendices 1-3)

1. Ndayisaba, A., Kaindlstorfer, C. & Wenning, G.K. Iron in Neurodegeneration - Cause or Consequence? *Front Neurosci* **13**, 180 (2019).
2. Li, K. & Reichmann, H. Role of iron in neurodegenerative diseases. *Journal of Neural Transmission* **123**, 389-399 (2016).
3. Viktorinova, A. & Durfinova, M. Mini-Review: Is iron-mediated cell death (ferroptosis) an identical factor contributing to the pathogenesis of some neurodegenerative diseases? *Neuroscience Letters* **745**, 135627 (2021).
4. Stephenson, J., Nutma, E., van der Valk, P. & Amor, S. Inflammation in CNS neurodegenerative diseases. *Immunology* **154**, 204-219 (2018).
5. Singh, A., Kukreti, R., Saso, L. & Kukreti, S. Oxidative Stress: A Key Modulator in Neurodegenerative Diseases. *Molecules* **24**(2019).
6. Kenkhuis, B. et al. Iron loading is a prominent feature of activated microglia in Alzheimer's disease patients. *Acta Neuropathologica Communications* **9**, 27 (2021).
7. Ayton, S. et al. Regional brain iron associated with deterioration in Alzheimer's disease: A large cohort study and theoretical significance. *Alzheimer's & Dementia* **17**, 1244-1256 (2021).
8. Deibel, M.A., Ehmann, W.D. & Markesbery, W.R. Copper, iron, and zinc imbalances in severely degenerated brain regions in Alzheimer's disease: possible relation to oxidative stress. *Journal of the Neurological Sciences* **143**, 137-142 (1996).
9. Craelius, W., Migdal, M.W., Luessenhop, C.P., Sugar, A. & Mihalakis, I. Iron deposits surrounding multiple sclerosis plaques. *Arch Pathol Lab Med* **106**, 397-9 (1982).
10. Hametner, S., Dal Bianco, A., Trattnig, S. & Lassmann, H. Iron related changes in MS lesions and their validity to characterize MS lesion types and dynamics with Ultra-high field magnetic resonance imaging. *Brain Pathol* **28**, 743-749 (2018).
11. Li, L.B. et al. Iron Exposure and the Cellular Mechanisms Linked to Neuron Degeneration in Adult Mice. *Cells* **8**(2019).
12. Dixon, S.J. et al. Ferroptosis: an iron-dependent form of nonapoptotic cell death. *Cell* **149**, 1060-72 (2012).
13. Stockwell, B.R. et al. Ferroptosis: A Regulated Cell Death Nexus Linking Metabolism, Redox Biology, and Disease. *Cell* **171**, 273-285 (2017).
14. Nnah, I.C., Lee, C.-H. & Wessling-Resnick, M. Iron potentiates microglial interleukin-1β secretion induced by amyloid-β. *Journal of Neurochemistry* **154**, 177-189 (2020).
15. Kenkhuis, B. et al. Iron accumulation induces oxidative stress, while depressing inflammatory polarization in human iPSC-derived microglia. *Stem Cell Reports* **17**, 1351-1365 (2022).
16. Cox, A.D., Fesik, S.W., Kimmelman, A.C., Luo, J. & Der, C.J. Drugging the undruggable RAS: Mission possible? *Nat Rev Drug Discov* **13**, 828-51 (2014).
17. Chen, Y. et al. Dexras1, a small GTPase, is required for glutamate-NMDA neurotoxicity. *J Neurosci* **33**, 3582-7 (2013).
18. Karlsson, M. et al. A single–cell type transcriptomics map of human tissues. *Science Advances* **7**, eabh2169.
19. Human Protein Atlas. Vol. 2022.
20. Xin, Y. et al. Dexras1 Induces Dysdifferentiation of Oligodendrocytes and Myelin Injury by Inhibiting the cAMP-CREB Pathway after Subarachnoid Hemorrhage. *Cells* **11**(2022).

21. Connor, J.R. & Menzies, S.L. Relationship of iron to oligodendrocytes and myelination. *Glia* **17**, 83-93 (1996).
22. Connor, J.R., Menzies, S.L., Burdo, J.R. & Boyer, P.J. Iron and iron management proteins in neurobiology. *Pediatr Neurol* **25**, 118-29 (2001).
23. Bartzokis, G. et al. MR evaluation of age-related increase of brain iron in young adult and older normal males. *Magn Reson Imaging* **15**, 29-35 (1997).
24. Ingrassia, R., Garavaglia, B. & Memo, M. DMT1 Expression and Iron Levels at the Crossroads Between Aging and Neurodegeneration. *Front Neurosci* **13**, 575 (2019).
25. Stephenson, E., Nathoo, N., Mahjoub, Y., Dunn, J.F. & Yong, V.W. Iron in multiple sclerosis: roles in neurodegeneration and repair. *Nature Reviews Neurology* **10**, 459-468 (2014).
26. Hametner, S. et al. Iron and neurodegeneration in the multiple sclerosis brain. *Annals of Neurology* **74**, 848-861 (2013).
27. Jhelum, P. et al. Ferroptosis Mediates Cuprizone-Induced Loss of Oligodendrocytes and Demyelination. *J Neurosci* **40**, 9327-9341 (2020).
28. Mercadante, A.A. & Tadi, P. Neuroanatomy, Gray Matter. in *StatPearls* (StatPearls Publishing
Copyright © 2022, StatPearls Publishing LLC., Treasure Island (FL), 2022).
29. Lieblein-Boff, J.C. et al. Neonatal E. coli infection causes neuro-behavioral deficits associated with hypomyelination and neuronal sequestration of iron. *J Neurosci* **33**, 16334-45 (2013).
30. Bergsland, N. et al. Targeting Iron Dyshomeostasis for Treatment of Neurodegenerative Disorders. *CNS Drugs* **33**, 1073-1086 (2019).
31. Rosenblum, S.L. & Kosman, D.J. Aberrant Cerebral Iron Trafficking Co-morbid With Chronic Inflammation: Molecular Mechanisms and Pharmacologic Intervention. *Front Neurol* **13**, 855751 (2022).
32. Fang, M. et al. Dexras1: a G protein specifically coupled to neuronal nitric oxide synthase via CAPON. *Neuron* **28**, 183-93 (2000).
33. Cheng, H.Y. et al. Dexras1 potentiates photic and suppresses nonphotic responses of the circadian clock. *Neuron* **43**, 715-28 (2004).
34. Cheah, J.H. et al. NMDA receptor-nitric oxide transmission mediates neuronal iron homeostasis via the GTPase Dexras1. *Neuron* **51**, 431-440 (2006).
35. Kemppainen, R.J. & Behrend, E.N. Dexamethasone rapidly induces a novel ras superfamily member-related gene in AtT-20 cells. *J Biol Chem* **273**, 3129-31 (1998).
36. Jaffrey, S.R., Fang, M. & Snyder, S.H. Nitrosopeptide mapping: a novel methodology reveals s-nitrosylation of dexras1 on a single cysteine residue. *Chem Biol* **9**, 1329-35 (2002).
37. Chen, Y., Mathias, L., Falero-Perez, J.M. & Kim, S.F. PKA-mediated phosphorylation of Dexras1 suppresses iron trafficking by inhibiting S-nitrosylation. *FEBS letters* **589**, 3212-3219 (2015).
38. Yan, N. & Zhang, J. Iron Metabolism, Ferroptosis, and the Links With Alzheimer's Disease. *Front Neurosci* **13**, 1443 (2019).
39. Dobson, R. & Giovannoni, G. Multiple sclerosis - a review. *Eur J Neurol* **26**, 27-40 (2019).
40. Robinson, A.P., Harp, C.T., Noronha, A. & Miller, S.D. The experimental autoimmune encephalomyelitis (EAE) model of MS: utility for understanding disease pathophysiology and treatment. *Handb Clin Neurol* **122**, 173-89 (2014).

41. Toomey, L.M. et al. Cuprizone feed formulation influences the extent of demyelinating disease pathology. *Scientific Reports* **11**, 22594 (2021).
42. Catanzaro, G. et al. Epigenetic modifications of Dexras 1 along the nNOS pathway in an animal model of multiple sclerosis. *J Neuroimmunol* **294**, 32-40 (2016).
43. Gao, H., Gao, Y., Li, X., Shen, A. & Yan, M. Spatiotemporal patterns of dexamethasone-induced Ras protein 1 expression in the central nervous system of rats with experimental autoimmune encephalomyelitis. *J Mol Neurosci* **41**, 198-209 (2010).
44. Liñares, D. et al. Neuronal nitric oxide synthase plays a key role in CNS demyelination. *The Journal of neuroscience : the official journal of the Society for Neuroscience* **26**, 12672-12681 (2006).
45. Khan, R.S. et al. Dexras1 Deletion and Iron Chelation Promote Neuroprotection in Experimental Optic Neuritis. *Sci Rep* **9**, 11664 (2019).
46. Karczewski, K.J. et al. The mutational constraint spectrum quantified from variation in 141,456 humans. *Nature* **581**, 434-443 (2020).
47. Graham, T.E., Key, T.A., Kilpatrick, K. & Dorin, R.I. Dexras1/AGS-1, a steroid hormone-induced guanosine triphosphate-binding protein, inhibits 3',5'-cyclic adenosine monophosphate-stimulated secretion in AtT-20 corticotroph cells. *Endocrinology* **142**, 2631-40 (2001).
48. Thapliyal, A., Verma, R. & Kumar, N. Small G Proteins Dexras1 and RHES and Their Role in Pathophysiological Processes. *Int J Cell Biol* **2014**, 308535 (2014).
49. Santos, A.I. et al. S-Nitrosylation of Ras Mediates Nitric Oxide-Dependent Post-Injury Neurogenesis in a Seizure Model. *Antioxid Redox Signal* **28**, 15-30 (2018).
50. Raines, K.W., Bonini, M.G. & Campbell, S.L. Nitric oxide cell signaling: S-nitrosation of Ras superfamily GTPases. *Cardiovascular Research* **75**, 229-239 (2007).
51. Doulias, P.-T. et al. Structural profiling of endogenous S-nitrosocysteine residues reveals unique features that accommodate diverse mechanisms for protein S-nitrosylation. *Proceedings of the National Academy of Sciences* **107**, 16958-16963 (2010).
52. Jumper, J. et al. Highly accurate protein structure prediction with AlphaFold. *Nature* **596**, 583-589 (2021).
53. Varadi, M. et al. AlphaFold Protein Structure Database: massively expanding the structural coverage of protein-sequence space with high-accuracy models. *Nucleic Acids Research* **50**, D439-D444 (2022).
54. Hallenbeck, K.K., Turner, D.M., Renslo, A.R. & Arkin, M.R. Targeting Non-Catalytic Cysteine Residues Through Structure-Guided Drug Discovery. *Curr Top Med Chem* **17**, 4-15 (2017).
55. Erlanson, D.A. et al. Site-directed ligand discovery. *Proceedings of the National Academy of Sciences of the United States of America* **97**, 9367-9372 (2000).
56. Small Molecule Discovery Center (SMDC): Technologies & Services. (UCSF School of Pharmacy Department of Pharmaceutical Chemistry, https://pharm.ucsf.edu/, 2022).
57. Hallenbeck, K.K. et al. A Liquid Chromatography/Mass Spectrometry Method for Screening Disulfide Tethering Fragments. *SLAS Discovery* **23**, 183-192 (2018).
58. Tamura, M. & Arata, Y. Expression, S-Nitrosylation, and Measurement of S-Nitrosylation Ratio of Recombinant Galectin-2. *Methods Mol Biol* **2132**, 55-63 (2020).
59. Mondal, S., Hsiao, K. & Goueli, S.A. A Homogenous Bioluminescent System for Measuring GTPase, GTPase Activating Protein, and Guanine Nucleotide Exchange Factor Activities. *Assay and drug development technologies* **13**, 444-455 (2015).

60. Joseph, S. et al. Myelinating glia-specific deletion of Fbxo7 in mice triggers axonal degeneration in the central nervous system together with peripheral neuropathy. *The Journal of Neuroscience*, 3094-18 (2019).
61. Fünfschilling, U. et al. Glycolytic oligodendrocytes maintain myelin and long-term axonal integrity. *Nature* **485**, 517-521 (2012).
62. Goebbels, S. et al. Genetic targeting of principal neurons in neocortex and hippocampus of NEX-Cre mice. *Genesis* **44**, 611-21 (2006).
63. Parkhurst, C.N. et al. Microglia promote learning-dependent synapse formation through brain-derived neurotrophic factor. *Cell* **155**, 1596-609 (2013).
64. Vanderlugt, C.L. et al. Pathologic Role and Temporal Appearance of Newly Emerging Autoepitopes in Relapsing Experimental Autoimmune Encephalomyelitis. *The Journal of Immunology* **164**, 670 (2000).
65. Constantinescu, C.S., Farooqi, N., O'Brien, K. & Gran, B. Experimental autoimmune encephalomyelitis (EAE) as a model for multiple sclerosis (MS). *Br J Pharmacol* **164**, 1079-106 (2011).
66. Rahn, E.J., Iannitti, T., Donahue, R.R. & Taylor, B.K. Sex differences in a mouse model of multiple sclerosis: neuropathic pain behavior in females but not males and protection from neurological deficits during proestrus. *Biology of sex differences* **5**, 4-4 (2014).
67. Abbasi, U., Abbina, S., Gill, A., Bhagat, V. & Kizhakkedathu, J.N. A facile colorimetric method for the quantification of labile iron pool and total iron in cells and tissue specimens. *Scientific Reports* **11**, 6008 (2021).
68. Kaech, S. & Banker, G. Culturing hippocampal neurons. *Nat Protoc* **1**, 2406-15 (2006).
69. Banker, G.A. & Cowan, W.M. Further observations on hippocampal neurons in dispersed cell culture. *Journal of Comparative Neurology* **187**, 469-493 (1979).
70. Vyas, Y., Montgomery, J.M. & Cheyne, J.E. Hippocampal Deficits in Amyloid-β-Related Rodent Models of Alzheimer's Disease. *Front Neurosci* **14**, 266 (2020).
71. Gong, Y. et al. Alzheimer's disease-affected brain: Presence of oligomeric Aβ ligands (ADDLs) suggests a molecular basis for reversible memory loss. *Proceedings of the National Academy of Sciences* **100**, 10417-10422 (2003).
72. Lacor, P.N. et al. Synaptic targeting by Alzheimer's-related amyloid beta oligomers. *J Neurosci* **24**, 10191-200 (2004).
73. Fontana, I.C. et al. Amyloid-β oligomers in cellular models of Alzheimer's disease. *Journal of Neurochemistry* **155**, 348-369 (2020).
74. De Felice, F.G. et al. Alzheimer's disease-type neuronal tau hyperphosphorylation induced by A beta oligomers. *Neurobiol Aging* **29**, 1334-47 (2008).
75. Brewer, G.J. & Cotman, C.W. Survival and growth of hippocampal neurons in defined medium at low density: advantages of a sandwich culture technique or low oxygen. *Brain Research* **494**, 65-74 (1989).
76. Brewer, G.J., Boehler, M.D., Jones, T.T. & Wheeler, B.C. NbActiv4 medium improvement to Neurobasal/B27 increases neuron synapse densities and network spike rates on multielectrode arrays. *J Neurosci Methods* **170**, 181-7 (2008).
77. Brewer, G.J., Torricelli, J.R., Evege, E.K. & Price, P.J. Optimized survival of hippocampal neurons in B27-supplemented Neurobasal, a new serum-free medium combination. *J Neurosci Res* **35**, 567-76 (1993).

78. Arnold, L.J., Dagan, A., Gutheil, J. & Kaplan, N.O. Antineoplastic activity of poly(L-lysine) with some ascites tumor cells. *Proceedings of the National Academy of Sciences* **76**, 3246-3250 (1979).
79. Aebersold, M.J. et al. Simple and Inexpensive Paper-Based Astrocyte Co-culture to Improve Survival of Low-Density Neuronal Networks. *Frontiers in Neuroscience* **12**(2018).
80. Iwata, M., Watanabe, S., Yamane, A., Miyasaka, T. & Misonou, H. Regulatory mechanisms for the axonal localization of tau protein in neurons. *Mol Biol Cell* **30**, 2441-2457 (2019).
81. Zempel, H., Thies, E., Mandelkow, E. & Mandelkow, E.M. Abeta oligomers cause localized Ca(2+) elevation, missorting of endogenous Tau into dendrites, Tau phosphorylation, and destruction of microtubules and spines. *J Neurosci* **30**, 11938-50 (2010).
82. Cline, E.N. et al. A novel crosslinking protocol stabilizes amyloid β oligomers capable of inducing Alzheimer's-associated pathologies. *J Neurochem* **148**, 822-836 (2019).